Gyrokinetic simulations of turbulent energy exchange in a dipole configuration

R. Numata[1]

[1] *Graduate School of Information Science, University of Hyogo, Kobe, Japan*

Introduction

Planetary magnetospheres and levitated ring dipole devices represent a unique class of plasma environments where high-temperature plasma is confined by strongly inhomogeneous magnetic fields. A defining characteristic of these environments is "entropy-mode" turbulence driven by magnetic curvature and pressure gradients. This turbulence is responsible for the "inward pinch" phenomenon [1, 2], where particles are transported against density gradients. Recent work in simplified Z-pinch configurations revealed that this turbulence can also drive a novel, collisionless thermal equilibration between species [3]. When the temperature ratio $\tau \equiv T_\mathrm{i}/T_\mathrm{e} \neq 1$, wave-particle resonances allow one species to carry negative energy, feeding the instability and facilitating a nonlinear energy exchange that pushes the system toward equal temperatures.

This study extends the investigation of this turbulent energy exchange to a three-dimensional dipole configuration. The key question addressed here is whether the collisionless energy-exchange mechanism found in Z-pinch geometry persists when field-line variation, trapped particles, and realistic dipole metrics are included. We present local linear and nonlinear gyrokinetic simulation results using the GS2 code to examine how these geometric factors influence the efficiency of collisionless thermal equilibration. Characterizing these processes helps clarify global self-organization and observed temperature profiles in magnetospheric and laboratory fusion plasmas.

Simulation Model

We consider electrostatic drift-type fluctuations in a low-beta plasma confined by a vacuum ring dipole generated by a ring coil. The vacuum magnetic flux in cylindrical coordinates (R, ϕ, Z) is

$$\bar{\Psi} = -\frac{1}{2\pi}\frac{4\bar{R}}{\sqrt{(1+\bar{R})^2+\bar{Z}^2}}\frac{(2-m)K(m)-2E(m)}{m} \tag{1}$$

where $m = 4\bar{R}/[(1+\bar{R})^2+\bar{Z}^2]$, and K and E are complete elliptic integrals. Lengths are normalized by the coil radius, and the flux is normalized so that the magnetic field at the origin is unity.

We take a flux tube specified by $0 < \rho_{\rm fl} = 1 - \bar{R} < 1$ and solve a local electrostatic gyrokinetic model for electrons and single-species ions. The field-line-following coordinates (ρ, α, θ) are constructed from $\boldsymbol{B} = \nabla\alpha \times \nabla\Psi(\rho) = B^{\theta}\boldsymbol{e}_{\theta}$. In the dipole configuration, there is no magnetic shear and $\alpha = -\phi$.

The background plasma is characterized by the Maxwellian distribution function,

$$f_s = n_s \left(\frac{m_s}{2\pi T_s}\right)^{3/2} \exp\left(-\frac{m_s v^2}{2T_s}\right) \tag{2}$$

where n_s, T_s, and m_s are the density, temperature, and mass, respectively. The subscript $s = \mathrm{i}, \mathrm{e}$ signifies the species. The background quantities at the specific position $\rho_{\rm fl}$ are denoted by a subscript 0, such as f_{0s}, n_{0s}, T_{0s}. The non-Boltzmann part h_s of the perturbed distribution, $\delta f_s = -(q_s\phi/T_{0s})f_{0s} + h_s$, evolves as

$$\frac{\partial h_s}{\partial t} + (v_{\parallel}\boldsymbol{b} + \boldsymbol{v}_{\mathrm{D},s} + \boldsymbol{v}_{E,s}) \cdot \nabla h_s = \left(\frac{\partial \langle\phi\rangle_{\boldsymbol{R}_s}}{\partial t} + \boldsymbol{v}^{\mathrm{T}}_{*,s} \cdot \nabla \langle\phi\rangle_{\boldsymbol{R}_s}\right) \frac{q_s f_{0s}}{T_{0s}} + C(h_s) \tag{3}$$

complemented by the quasi-neutrality condition determining the electrostatic potential ϕ,

$$\sum_s q_s \delta n_s = 0, \tag{4}$$

where $\delta n_s = \int \delta f_s dv$, q_s is the charge, and $\mathbf{v}_{D,s}$, $\mathbf{v}^{T}_{*,s}$, and $\mathbf{v}_{E,s} = \mathbf{b} \times \nabla\langle\phi\rangle_{\mathbf{R}_s}/B(\theta)$ are the magnetic, diamagnetic, and $E \times B$ drift velocities. The brackets denote gyro-averaging, and $C(h_s)$ represents collisions.

We decompose the fluctuations as $h_s = \sum_{\mathbf{k}} h_{\mathbf{k},s} e^{iS}$ and $\phi = \sum_{\mathbf{k}} \phi_{\mathbf{k}} e^{iS}$, where $S = k_x X + k_y Y$. The local Cartesian coordinates are

$$\frac{x}{\rho_{\rm N}} = \frac{X}{L_{\rm N}} = \left.\frac{\mathrm{d}\hat{\Psi}}{\mathrm{d}\rho}\right|_{\rm fl} \rho, \qquad\qquad \frac{y}{\rho_{\rm N}} = \frac{Y}{L_{\rm N}} = \left.\frac{\mathrm{d}\hat{\Psi}}{\mathrm{d}\rho}\right|_{\rm fl} \alpha. \tag{5}$$

where $B_{\rm N}$, $\rho_{\rm N}$, and $L_{\rm N}$ are the reference magnetic field, Larmor radius, and macroscopic magnetic-field scale. The normalized flux is $\hat{\Psi} = \Psi/(L_N^2 B_N)$ and $\boldsymbol{k} = \nabla S$.

The magnetic and diamagnetic drift frequencies are given by

$$\omega_{\mathrm{D},s} = \omega_{\kappa,s}\frac{v_{\parallel}^2}{v_{\mathrm{th},s}^2} + \omega_{\nabla B,s}\frac{v_{\perp}^2}{2v_{\mathrm{th},s}^2}, \qquad\qquad \omega^{\mathrm{T}}_{*,s} = \omega_{*,n,s}\left(1 + \eta_s\left(\frac{v^2}{v_{\mathrm{th},s}^2} - \frac{3}{2}\right)\right) \tag{6}$$

where $v_{\mathrm{th},s} = \sqrt{2T_{0s}/m_s}$ and the velocity-independent drift frequencies are, respectively, given by

$$\omega_{\kappa,s} = \frac{2k_y T_{0s}}{q_s \mathsf{R} L_{\rm N} B_{\rm N}}, \qquad \omega_{\nabla B,s} = \frac{2k_y T_{0s}}{q_s \ell_B L_{\rm N} B_{\rm N}}, \qquad \omega_{*,n,s} = \frac{k_y T_{0s}}{q_s \ell_{n,s} L_{\rm N} B_{\rm N}}, \tag{7}$$

$$\frac{1}{\mathsf{R}} = (\boldsymbol{b}\cdot\nabla\boldsymbol{b})\cdot\boldsymbol{e}_{\rho}, \qquad \frac{1}{\ell_B} = -\frac{1}{B}\nabla B\cdot\boldsymbol{e}_{\rho}, \qquad \frac{1}{\ell_{n,s}} = -\frac{1}{n_s}\nabla n_s\cdot\boldsymbol{e}_{\rho}. \tag{8}$$

The ratio of the density and temperature gradient scale lengths is $\eta_s = \ell_{n,s}/\ell_{T,s}$.

We also introduce the parameter d_s, which measures the ratio of diamagnetic to magnetic drift,

$$d_s \equiv \left\langle 4\frac{\omega_{*,n,s}+\omega_{*,T,s}}{\omega_{\nabla B,s}+\omega_{\kappa,s}} \right\rangle_\theta . \tag{9}$$

The angle bracket $\langle\rangle_\theta$ is the flux-surface average. For low beta, $\ell_B = R$, and (9) reduces to $d_s = (1+\eta_s)\mathrm{R}/\ell_{n,s}$.

Simulation Results

We first examine the dependence of the linear eigenvalues on the flux-tube location $\rho_{\rm fl}$. In the limit $\rho_{\rm fl} \to 0$, the field line becomes circular and the Z-pinch limit is recovered. Figure 1 shows collisionless results for $d_s = 2$, $\eta_s = 0$, $m_{\rm i}/m_{\rm e} = 100$, and $\tau = 1$. The wavenumber is normalized by the ion sound Larmor radius for the outboard magnetic field $\rho_{\rm Se} = \sqrt{m_{\rm i}T_{0\rm e}}/(q_{\rm i}B_{\rm out})$, the time scale is normalized by $\langle R_{\rm c}\rangle_\theta/v_{\rm th,i}$ where $R_{\rm c} = \mathrm{R}L_{\rm N}$ is the curvature radius. We observe that the eigenvalues converge to the Z-pinch values as $\rho_{\rm fl} \to 0$. Interestingly, the real frequency changes sign as $\rho_{\rm fl}$ increases, suggesting a change in the dominant resonant species and hence in the direction of collisionless energy flow.

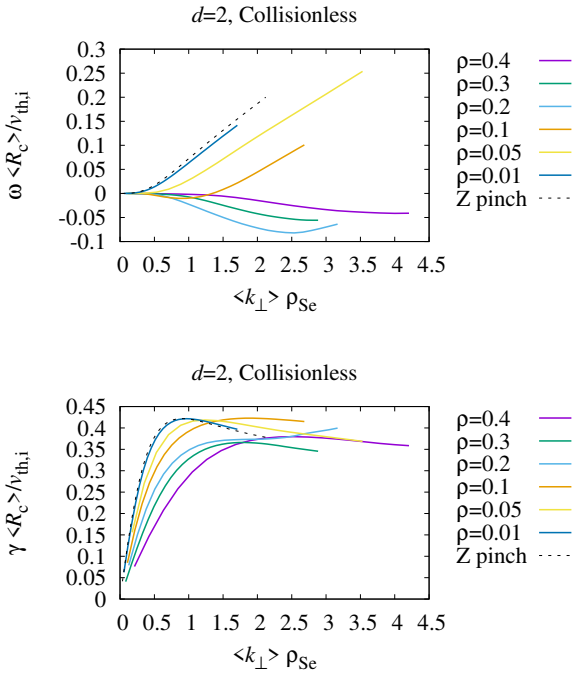

Figure 1: Collisionless linear eigenvalues for $d_s = 2$. Top: real frequency; bottom: growth rate. Dashed curves show the Z-pinch limit.

We next perform nonlinear simulations to examine turbulent transport and energy exchange. We set the simulation domain as $L_{x,y}/\rho_{\rm i} = 32\pi$ and the numerical resolution $N_{x,y} = 128$, $N_\lambda = 16 + N_\theta/2$ (for passing and trapped particles), $N_E = 32$, and N_θ ranging from 32 to 160 according to the magnetic field variation along the field line. The higher resolution along the field line is needed to suppress numerical instability. The collision frequency is $\nu_s\langle R_{\rm c}\rangle_\theta/v_{\rm th,i} = 0.01$. As in [3], we include hyper-viscosity.

Figure 2 shows the particle flux and energy exchange for different $\rho_{\rm fl}$. At fixed driving strength d_s, the particle flux decreases with increasing $\rho_{\rm fl}$, although the linear growth rate varies

only weakly. A similar trend is observed for the energy exchange. For $\tau = 1$, the ion heating is nearly zero at $\rho_{\rm fl} = 0.2$, whereas for $\tau = 2$ ($\tau = 0.5$) it has a finite negative (positive) value. This indicates cooling of the hotter species, consistent with thermal equilibration in the Z-pinch case.

So far, nonzero ion heating/cooling has been observed only in a limited set of parameter cases; a broader parameter scan is needed to characterize energy exchange in dipole plasmas.

Conclusion

We have performed linear and nonlinear gyrokinetic simulations of dipole plasmas to investigate turbulent transport and inter-species energy exchange. The linear analysis shows that, as the flux-tube location $\rho_{\rm fl}$ approaches zero, the eigenvalues converge to the circular Z-pinch limit. The real frequency changes sign as $\rho_{\rm fl}$ increases, suggesting a change in the dominant destabilizing species and in the direction of collisionless energy flow driven by wave-particle resonances.

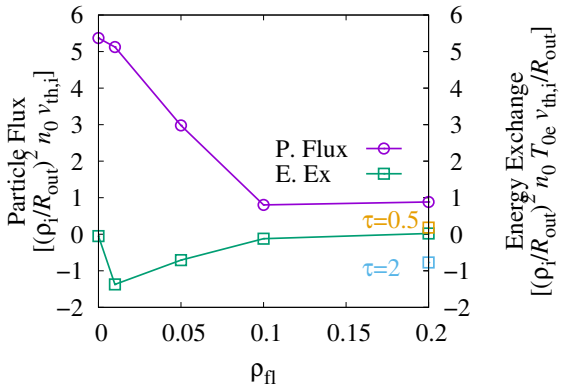

Figure 2: Nonlinear particle flux and inter-species energy exchange versus flux-tube location $\rho_{\rm fl}$ for $d_s = 2$. Negative ion heating for $\tau = 2$ and positive ion heating for $\tau = 0.5$ indicate cooling of the hotter species.

The nonlinear simulations show that, for fixed driving strength d_s, both the particle flux and the inter-species energy exchange decrease as $\rho_{\rm fl}$ increases, even though the linear growth rate remains relatively unchanged. For the $\tau = 2$ and $\tau = 0.5$ cases examined here, finite ion cooling and heating are observed, respectively, indicating cooling of the hotter species and relaxation toward thermal equilibration, consistent with the Z-pinch result. Since this behavior has so far been observed only in a limited parameter set, more comprehensive simulations are needed to clarify global transport and self-organization in dipole configurations.

References

[1] S. Kobayashi, B. N. Rogers, and W. Dorland, Phys. Rev. Lett., **103**, 055003 (2009).

[2] S. Kobayashi, B. N. Rogers, and W. Dorland, Phys. Rev. Lett., **105**, 235004 (2010).

[3] R. Numata, Mon. Not. R. Astron. Soc. Lett. **538**, L94-L99 (2025).